Criticality in coupled quantum spin chains with competing ladderlike and two-dimensional couplings: Contrasting $SrCu_2O_3$ with $CaCu_2O_3$

Pinaki Sengupta,[1,*] Weihong Zheng,[2,†] and Rajiv R. P. Singh[1,‡]
[1]*Department of Physics, University of California, Davis, California 95616, USA*
[2]*School of Physics, University of New South Wales, Sydney, NSW 2052, Australia*
(Received 10 September 2003; revised manuscript received 18 November 2003; published 26 February 2004)

Motivated by the geometry of spins in the materials $SrCu_2O_3$ and $CaCu_2O_3$, we study a two-layer, spin-half Heisenberg model, with nearest-neighbor exchange couplings J and αJ along the two axes in the plane and a coupling $J_\perp$ perpendicular to the planes. We study these class of models using the stochastic series expansion quantum Monte Carlo simulations at finite temperatures and series expansion methods at $T=0$. The critical value of the interlayer coupling, $J_\perp^c$, separating the Néel ordered and disordered ground states, is found to follow very closely a square root dependence on α. Both $T=0$ and finite-temperature properties of the model are presented and the contrasting behavior of $SrCu_2O_3$ and $CaCu_2O_3$ are explained.

DOI: 10.1103/PhysRevB.69.064428 PACS number(s): 75.40.Gb, 75.40.Mg, 75.10.Jm, 75.30.Ds

I. INTRODUCTION

In recent years, the geometrical arrangement of atoms carrying spin and those mediating interactions between them, in newly discovered magnetic materials, has been a dominant theme in the field of quantum magnetism, and has inspired many interesting models and theories.[1] In a class of cuprate materials, the arrangement of copper and oxygen atoms in the copper-oxide planes leads to nearly ideal realizations of one-dimensional (1D) spin chains, of spin ladders as well as of simple and decorated square-lattice systems.[2,3] The variations in geometry, in other recently discovered materials, have led to several magnetically ordered, spin-gapped and dimerized phases.[4] These materials have allowed the exploration of dimensional crossovers, unusual excitations, and quantum critical phenomena[5,6] through detailed comparisons between experiments and theory.

Many classes of materials involve weakly coupled spin-half chains. From a theoretical point of view, these are ideal systems for finding and testing novel phenomena as our understanding of the spin-half chain is rather complete thanks to Bethe ansatz methods, quantum field-theory methods, and numerical techniques.[7–9] However, different ways of coupling the chains together can lead to widely different behaviors. If two Heisenberg chains are coupled weakly together, it is known to lead to a disordered ground state and a gap in the spin-excitation spectra. These systems have been called spin ladders and are considered generic examples of spin gap phenomena.[2,10] On the other hand, if an array of spin chains, say arranged parallel to each other in a two-dimensional plane, are weakly coupled together in an unfrustrated manner, they develop conventional Néel order.[11] If the interchain couplings are strongly frustrated, one can even find a carry-over of exotic one-dimensional physics to higher dimensions.[12,13]

In this paper, we are motivated by the material $CaCu_2O_3$, which has a geometry very similar to the well-known spin-ladder material $SrCu_2O_3$, but develops Néel order at low temperatures.[14] The largest exchange coupling in both these materials is of order 2000 K. One can regard these materials as spin chains coupled in two different ways. Along one axis perpendicular to the chains, one has effectively a two-leg ladder, which are then nearly decoupled from the rest of the system, due to the geometry of copper-oxygen bond angles. Along the other axis perpendicular to the chains, the coupling between the chains leads to an anisotropic square lattice of spins.[15] Thus the materials have competing tendencies to Néel order and to develop a gap in the spin excitation spectra. The material $SrCu_2O_3$ is known to have a spin gap.[16] Néel order is found[14] in bulk $CaCu_2O_3$ materials with $T_N = 25$ K. Schön *et al.*[17] have also argued that thin films of $CaCu_2O_3$ act as spin ladders and show field-induced superconducitvity. While controversy surrounding the work of Schön *et al.* puts the existence of field-induced superconductivity in doubt, the fact remains that these materials are close to being quantum critical and could go into an ordered or disordered phase with small changes in parameters.

Here we consider two square-lattice layers of spins, with axes of the square lattice pointing along x and y and a Heisenberg Hamiltonian

$$\mathcal{H} = J\sum_{a,i} S_{a,i}S_{a,i+\hat{x}} + \alpha J\sum_{a,i} S_{a,i}S_{a,i+\hat{y}} + J_\perp \sum_i S_{1,i}S_{2,i}. \tag{1}$$

Here, a takes values 1 and 2, the first sum runs over the nearest neighbors along the x axis, the second over the nearest neighbor along the y axis and the third between the nearest neighbors along the z axis. The model $\mathcal{H}$, in the limit of $\alpha=1$ (the isotropic bilayer), has been extensively studied using numerical and analytical methods.[18] We shall call $\mathcal{H}$ an anisotropic bilayer model. We set $J=1$ and study the phase diagram of this model at $T=0$ using series expansion methods and stochastic series expansion (SSE) quantum Monte Carlo (QMC) simulations. We find that the phase boundary separating the Néel ordered and disordered phases follows very closely the behavior

$$J_\perp^c = A\sqrt{\alpha}, \tag{2}$$

TABLE I. Series coefficients for dimer expansions of the ground-state energy per site $E_0/NJ_\perp$, the antiferromagnet susceptibility χ, the minimum triplet energy gap $m/J_\perp$, and the critical spin-wave velocity along the x and y directions (as described in the text). Coefficients of $(J/J_\perp)^n$ for $\alpha=1/2$ up to order $n=11$ are listed.

n	$E_0/J_\perp$	χ	$m/J_\perp$	$2CD_x/J_\perp^2$	$2CD_y/J_\perp^2$
0	$-3.750000000\times10^{-1}$	1.000000000	1.000000000	0.000000000	0.000000000
1	0.000000000	3.000000000	-1.500000000	1.000000000	5.000000000×10^{-1}
2	$-2.343750000\times10^{-1}$	7.125000000	1.250000000×10^{-1}	0.000000000	0.000000000
3	$-1.054687500\times10^{-1}$	1.546875000×10^{1}	$-4.687500000\times10^{-1}$	1.750000000	5.468750000×10^{-1}
4	$-2.270507813\times10^{-2}$	3.132617187×10^{1}	$-5.078125000\times10^{-1}$	1.218750000	1.757812500×10^{-1}
5	8.184814453×10^{-2}	6.153011068×10^{1}	$-1.647949219\times10^{-1}$	$-4.101562500\times10^{-1}$	$-3.376464844\times10^{-1}$
6	9.038543701×10^{-2}	1.188306387×10^{2}	2.856903076×10^{-1}	-1.158325195	$-1.558227539\times10^{-1}$
7	1.045632362×10^{-2}	2.276296512×10^{2}	7.159423828×10^{-2}	-1.660129547	$-8.045387268\times10^{-2}$
8	$-1.300574541\times10^{-1}$	4.326861726×10^{2}	$-8.715667129\times10^{-1}$	6.815385818×10^{-1}	7.272934914×10^{-1}
9	$-1.566342926\times10^{-1}$	8.165576512×10^{2}	-2.380170342	3.975312367	8.960766308×10^{-1}
10	$-2.075107419\times10^{-2}$	1.529763646×10^{3}	-1.890960221	2.580596185	$-2.333164847\times10^{-1}$
11	2.349058435×10^{-1}	2.850279307×10^{3}	$-1.916425429\times10^{-1}$	-2.162085212	-1.298405600

where $A\approx2.53$ is the critical point for isotropic case. We also calculate the uniform susceptibility and the internal energy of the model at finite temperatures, and study its excitation spectra in the spin-gap and Néel ordered phases.

The plan of the paper is as follows. In Sec. II, we discuss the series expansion method. In Sec. III, we discuss the stochastic series expansion calculations. In Sec. IV, we present the $T=0$ properties of the system. In Sec. V, we present the uniform susceptibility and internal energy at finite temperatures and in Sec. VI, we present our conclusions.

II. SERIES EXPANSION METHODS

We have carried out dimer expansions and Ising expansions for this system at $T=0$. The linked-cluster series expansion method has been previously reviewed in Ref. 19, and will not be repeated here.

A. Dimer expansions

In the limit that the exchange coupling along the rung $J_\perp$ is much larger than the couplings within the plane, the rungs interact only weakly with each other, and the dominant configuration in the ground state is the product state with the spin on each rung forming a spin singlet. We can construct dimer expansion in $J/J_\perp$ by treating the last term in Eq. (1) as the unperturbed Hamiltonian and the rest of terms as a perturbation.

We have carried out the dimer expansions for the $T=0$ ground-state energy per site E_0/N, the antiferromagnetic susceptibility χ, and the lowest lying triplet excitation spectrum $\Delta(k_x,k_y)$ (odd parity under interchange of the planes) up to order $(J/J_\perp)^{11}$ for fixed values of α. The resulting power series in $J/J_\perp$ for the ground-state energy per site E_0/N and the antiferromagnetic susceptibility χ for $\alpha=1/2$ are presented in Table I. A table of series coefficients for the triplet excitation spectrum $\Delta(k_x,k_y)$ would require an inordinate amount of space to reproduce in print; it is available from the authors upon request. Instead, we also present in Table I the series for the minimum energy gap $m=\Delta(\pi,\pi)$. The dimer expansion for isotropic case ($\alpha=1$) was carried out by Hida[20] up to order $(J/J_\perp)^6$ in 1992, and extended to order $(J/J_\perp)^8$ by Gelfand,[21] and to order $(J/J_\perp)^{11}$ by one of the authors.[22] Here, the number of clusters involved is much more than the isotropic case since the system no longer has 90° rotation symmetry, and there are, in all, 38 070 linked clusters of up to 12 sites involved in the calculation.

B. Ising expansions

To construct an expansion about the Ising limit for this system, one has to introduce an anisotropy parameter x, and write the Hamiltonian for Heisenberg-Ising model as

$$H=H_0+xV, \tag{3}$$

where

$$\begin{aligned} H_0 &= J\sum_{a=1,2}\sum_i S^z_{a,i}S^z_{a,i+\hat{x}}+\alpha J\sum_{a=1,2}\sum_i S^z_{a,i}S^z_{a,i+\hat{y}} \\ &\quad + J_\perp\sum_i S^z_{1,i}S^z_{2,i}+t\sum_{\alpha,i}\epsilon_{\alpha,i}S^z_{\alpha,i}, \\ V &= J\sum_{\alpha=1,2}\sum_i (S^x_{\alpha,i}S^x_{\alpha,i+\hat{x}}+S^y_{\alpha,i}S^y_{\alpha,i+\hat{x}}) \\ &\quad + \alpha J\sum_{\alpha=1,2}\sum_i (S^x_{\alpha,i}S^x_{\alpha,i+\hat{y}}+S^y_{\alpha,i}S^y_{\alpha,i+\hat{y}}) \\ &\quad + J_\perp\sum_i (S^x_{1,i}S^x_{2,i}+S^y_{1,i}S^y_{2,i})-t\sum_{\alpha,i}\epsilon_{\alpha,i}S^z_{\alpha,i}, \end{aligned} \tag{4}$$

and $\epsilon_{\alpha,i}=\pm1$ on the two sublattices. The last term in both H_0 and V is a local staggered field term, which can be included to improve convergence. The limits $x=0$ and $x=1$ correspond to the Ising model and the isotropic Heisenberg model, respectively. The operator H_0 is taken as the unperturbed Hamiltonian, with the unperturbed ground state being

the usual Néel state. The operator V is treated as a perturbation. It flips a pair of spins on neighboring sites.

The Ising series have been calculated for the ground state energy per site E_0/N, the staggered magnetization M, the uniform perpendicular susceptibility $\chi_\perp$, and the lowest lying triplet excitation spectrum $\Delta(k_x,k_y,k_z)$ for several ratio of couplings and (simultaneously) for several values of t up to order x^{10} (the series for uniform perpendicular susceptibility $\chi_\perp$ is one order less). The series are available upon request. Here there are two branches of the spin-wave dispersion. From the series one can see that the symmetric (optical) excitation spectrum $\Delta(k_x,k_y,0)$ is related to the antisymmetric (acoustic) excitation spectrum $\Delta(k_x,k_y,\pi)$ by

$$\Delta(k_x,k_y,0)=\Delta(\pi-k_y,\pi-k_x,\pi), \tag{5}$$

and so we only consider the antisymmetric excitation spectrum here.

III. QUANTUM MONTE CARLO SIMULATIONS

We have used the stochastic series expansion (SSE) method[23,24] to study the ground state and finite temperature properties of the Heisenberg antiferromagnet on anisotropic bilayers. The SSE is a finite-temperature QMC technique based on importance sampling of the diagonal matrix elements of the density matrix $e^{-\beta H}$. Ground-state properties are obtained by using sufficiently large values of β. There are no approximations beyond statistical errors. Using the ''operator-loop'' cluster update,[24] the autocorrelation time for the system sizes we consider here (up to $\approx\times 10^3$ spins) is at most a few Monte Carlo sweeps even at the critical coupling.[25]

IV. $T=0$ PROPERTIES

A. Results from dimer expansions

With the dimer series for the antiferromagnetic susceptibility χ, and the minimum triplet gap m, one can determine the critical point $(J/J_\perp)_c$ by constructing Dlog Padé approximants[26] to these series, and since the transition should lie in the universality class of the classical $d=3$ Heisenberg model (our unbiased analysis also supports this), we expect that the critical index for χ and m should be approximately 1.40 and 0.71, respectively. The critical line obtained by the exponent-biased Dlog Padé approximants[21] are shown in Fig. 1.

The spectra for some particular values of α and $J/J_\perp$ in the dimer phase are illustrated in Fig. 2, where the direct sum to the series at $J/J_\perp=(J/J_\perp)_c$ is indeed consistent with the integrated differential approximants[21] that one can construct. In Fig. 3, we show the spectra for some particular values of α and $J/J_\perp$ along the critical line.

To compute the critical spin-wave velocity v, one expands the spectrum Δ in the vicinity of wave vector (π,π) up to $\mathbf{k}^2$:

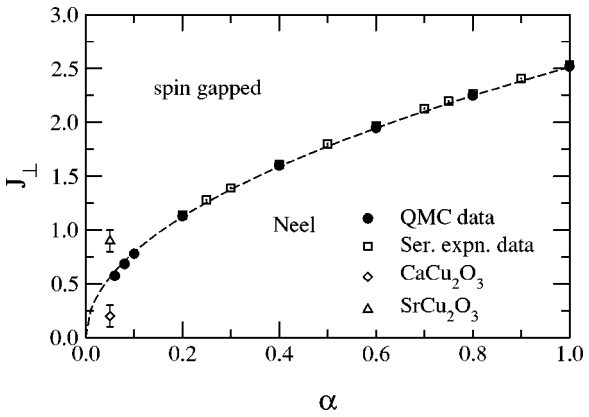

FIG. 1. The ground-state phase diagram in the parameter space of the in-plane anisotropy α and the interlayer coupling $J_\perp$. Both QMC and series expansion results are shown. The error bars are smaller than the size of the symbols. The curve is a square root fit to the critical coupling data. Rough estimates of parameters for $CaCu_2O_3$ and $SrCu_2O_3$ are also indicated.

$$\Delta(\pi-k_x,\pi-k_y)(J/J_\perp) = C(J/J_\perp)+D_x(J/J_\perp)k_x^2+D_y(J/J_\perp)k_y^2+\cdots, \tag{6}$$

and it is easy to prove[21] that the critical spin-wave velocity along the x and y direction are equal to $(2CD_x)^{1/2}$ and $(2CD_y)^{1/2}$, respectively, at $(J/J_\perp)_c$. The series coefficients for $2CD_x$ and $2CD_y$ in $J/J_\perp$ are listed in Table I. These series can be extrapolated to $(J/J_\perp)_c$ by using the integrated differential approximants, and the results are shown in Fig. 4, one can see that v_x (v_y) is increased (decreased) once the anisotropy is introduced. As $\alpha\to 0$, near the critical line $J_\perp$

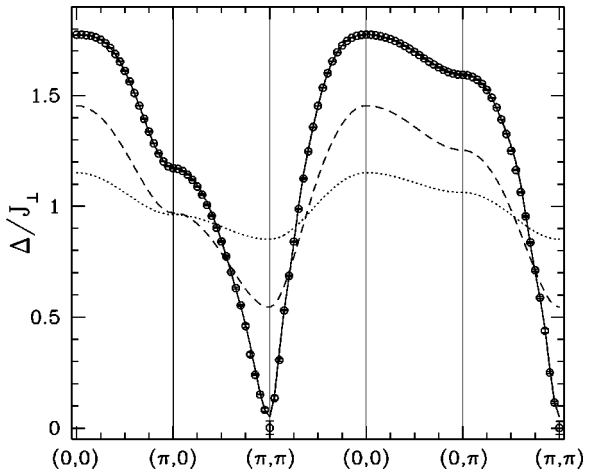

FIG. 2. Plot of the antisymmetric spin-triplet excitation spectrum $\Delta(k_x,k_y,\pi)/J_\perp$ in the dimer phase along high-symmetry cuts through the Brillouin zone for the system with coupling ratios $\alpha=0.5$ and $J/J_\perp=0.1$ (dotted line), 0.3 (dashed line), 0.556 (solid line). The lines are the estimates by direct sum to the dimer series, and the points circles with error bar for the case of $J/J_\perp=0.556$ only are the estimates of the integrated differential approximants to the dimer series.

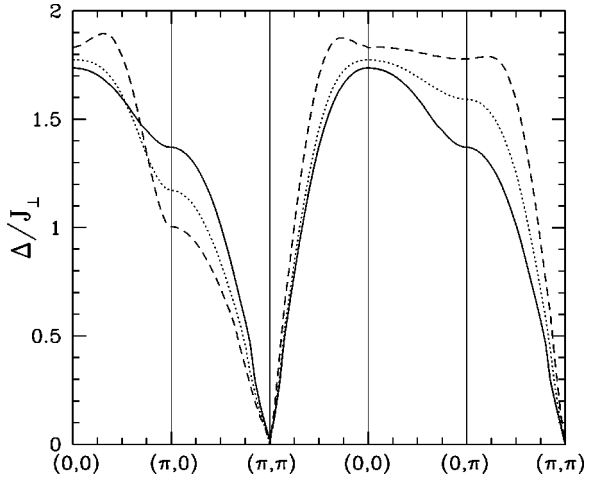

FIG. 3. Plot of the antisymmetric spin-triplet excitation spectrum $\Delta(k_x,k_y,\pi)/J_\perp$ along high-symmetry cuts through the Brillouin zone for the system along the critical line with $\alpha=0.25$ (dashed line), 0.5 (dotted line), 1(solid line). The results of the integrated differential approximants to the dimer series are shown.

$\rightarrow 0$ and the system approaches a spin-chain along the x axis, where the spin-wave velocity is known to be $\pi J/2$. Hence asymptotically, along the critical line,

$$v_x/J_\perp \simeq (\pi/2)(J/J_\perp) \sim 0.619/\sqrt{\alpha}. \tag{7}$$

This asymptotic behavior is shown by a dashed line. One can see that the presence of other interactions further increases the spin-wave velocity along x. To understand the behavior of v_y, we turn to linear spin-wave theory. We obtain the antisymmetric excitation spectrum

$$\Delta(k_x,k_y) = 2SJ\{(1+\alpha+J_\perp/2J)^2 - [\cos(k_x)+\alpha\cos(k_y)-J_\perp/2J]^2\}^{1/2} \tag{8}$$

with this one can obtain spin-wave velocity along the y direction

$$v_y = 2SJ[\alpha(1+\alpha+J_\perp/J)]^{1/2}. \tag{9}$$

Note that v_x is obtained from v_y by exchanging the intralayer couplings along the x and y directions. The linear spin-wave results for both v_x and v_y are plotted as dotted lines in Fig. 4. We see that for small α, the linear spin-wave theory, which is known to be off by a factor of $\pi/2$ for the spin-half chain, works quite well for v_y, the velocity along the weakly coupled direction.

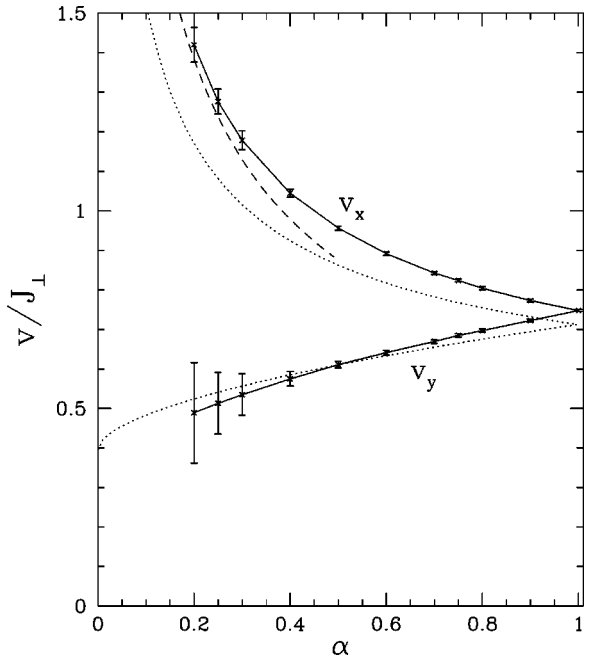

FIG. 4. The spin-wave velocity $v/J_\perp$ along x and y directions versus α at the critical ratio $(J/J_\perp)_c$ obtained from dimer series expansion. Also shown are the asymptotic results of $v_x/J_\perp = 0.619/\sqrt{\alpha}$ (dashed line) and the linear spin-wave results for v_x and v_y (dotted lines).

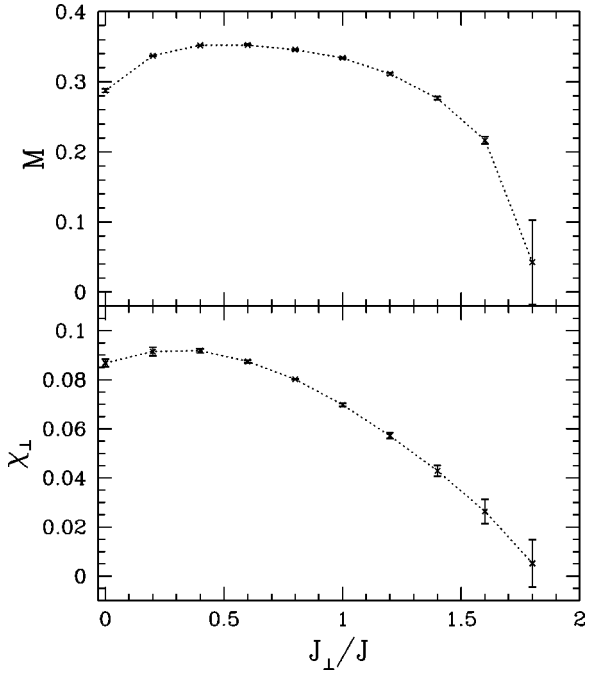

FIG. 5. The staggered magnetization M and the uniform perpendicular susceptibility $\chi_\perp$ vs $J_\perp/J$ for $\alpha=0.5$ as estimated by Ising expansions.

B. Results from Ising expansions

With the Ising series for staggered magnetization M and the uniform perpendicular susceptibility $\chi_\perp$, one can also determine the phase boundary by extrapolating the series for M and $\chi_\perp$ to the isotropic point $x=1$ using the same method as in Ref. 22, the results for $\alpha=1/2$ are shown in Fig. 5. We note that M and $\chi_\perp$ first increase for small $J_\perp/J$, then decrease for a larger value of $J_\perp/J$, and vanish at about $J_\perp/J = 1.8$, which is consistent with the more accurate critical point determined by the dimer expansions. The reason for the initial increase is that for small $J_\perp/J$ the interlayer coupling

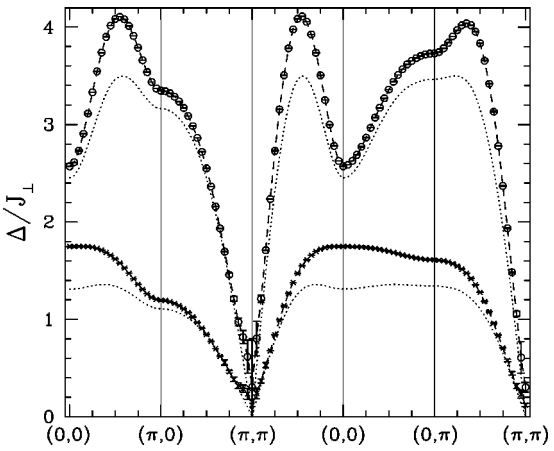

FIG. 6. Plot of the antisymmetric spin-triplet excitation spectrum $\Delta(k_x,k_y,\pi)/J_\perp$ in the Néel order phase derived from the Ising expansions along high symmetry cuts through the Brillouin zone for the system with coupling ratios $\alpha=0.5$ and $J_\perp/J=0.5$ (upper curve), 1.75 (lower curve), also shown as dotted lines are the results of linear spin-wave theory.

enhances the antiferromagnetic long-range order as the system acquires a weak three dimensionality and quantum fluctuations are suppressed.

The antisymmetric excitation spectra $\Delta(k_x,k_y,\pi)$ for some particular values of $J_\perp/J$ and $\alpha=1/2$ are illustrated in Fig. 6, where we can see that the excitation is gapless at the (π,π,π) point. For $J_\perp/J=1.75$ (close to the critical point), the spectra are very similar to that obtained from dimer expansion. Thus, as one goes through the quantum phase transition, the spectra evolve smoothly.

C. Ground-state properties obtained by SSE

For the ground-state properties, using the SSE method, we have studied lattices of the form $2\times L\times L$, with L up to 20. Periodic boundary conditions were applied in both the x and y directions. A series of values of α were chosen, and the critical $J_\perp$ was determined for each of them, mapping out the ground-state phase diagram in the $\alpha-J_\perp$ parameter space. An inverse temperature $\beta=16L$ was found to be sufficient for the calculated quantities to have converged to their ground-state values.

An efficient way to determine the critical coupling for the spin gap transition is by studying the finite size scaling of the ground-state $(T=0)$ spin stiffness. The spin stiffness can be defined[27,28] as the second derivative of the free energy with respect to a uniform twist ϕ. At $T=0$, the free energy is the same as the internal energy, and the expression for the spin stiffness takes the form

$$\rho=\frac{\partial^2 E(\phi)}{\partial\phi^2}, \tag{10}$$

where $E(\phi)$ is the internal energy per spin in the presence of a twist. The stiffness can be related to the fluctuations of the ''winding number'' in the simulations[23,29–31] and hence can be estimated directly without actually including a twist.

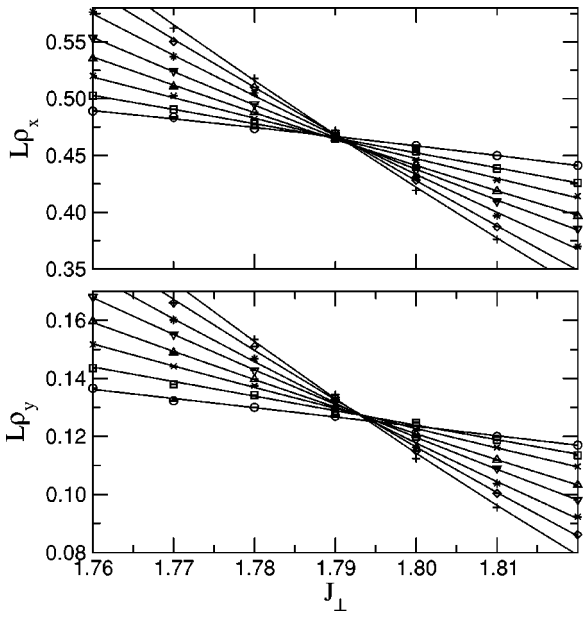

FIG. 7. The ground-state spin stiffness times the linear system size L as a function of the interlayer coupling in the vicinity of the critical point for square lattices with $L=6,8,\ldots,20$. The (negative) slope increases with increasing L. The intralayer anisotropy is $\alpha=0.5$. The upper (lower) panel shows the data for stiffness along the x (y) axis. Error bars are of the size of the symbols or smaller. The curves are quadratic fits to the data.

Since the twist can be applied parallel to the x or y axes, there are two different spin stiffnesses ρ_x and ρ_y in the anisotropic system considered here.

Finite size scaling analysis dictates that at the critical coupling, the spin stiffness should scale with the system size as[32,33]

$$\rho(L)\sim L^{d-2-z}, \tag{11}$$

where $d(=2)$ is the dimensionality and z is the dynamical critical exponent. The transition is expected to be in the universality class of the 3D Heisenberg model—hence $z=1$. It follows from the above relation that in a plot of $L\rho_\alpha,(\alpha=x,y)$ versus $J_\perp$, the curves for different system size should intersect at $J_\perp^c$. In practice, it is found that the crossing point shifts monotonically with increasing system size—the intersection of the curves for successive system sizes (linear dimensions L and $L+2$) give a finite size dependent estimate of the critical coupling $J_\perp^c(L)$ that converges to the true critical coupling $J_\perp^c$ at large L. Interestingly, the convergence is from opposite directions for ρ_x and ρ_y—$J_\perp^c(L)\to J_\perp^c$ from above (below) for $\rho_y(\rho_x)$.[34] This yields upper and lower bounds for the true critical coupling, leading to an improved estimate for $J_\perp^c$. The results for $\alpha=0.5$ are shown in Fig. 7. The upper (lower) panel shows the data for $\rho_x(\rho_y)$. The curves are found to cross in the neighborhood of $J_\perp\approx 1.8$. A plot of the finite size dependent critical coupling obtained from the crossing of successive system sizes obtained from the plot is shown in Fig. 8. As discussed above, $J_\perp^c(L)$ is seen to converge toward ≈ 1.79 from above (below) for

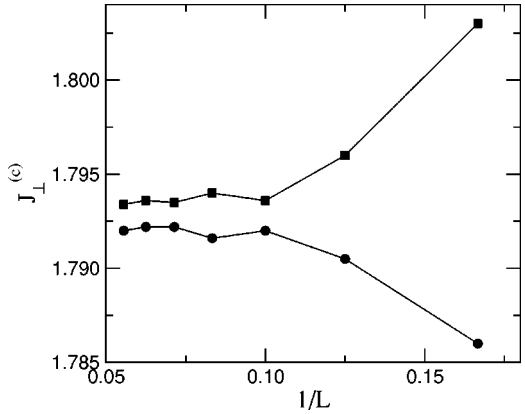

FIG. 8. The finite-size dependent critical point as obtained from the crossing of the stiffness curves for successive system sizes with linear dimensions L and $L+2$. The estimate for the critical coupling converges from above (below) for the $\rho_y(\rho_x)$ data, providing upper and lower bounds for the true critical coupling in the thermodynamic limit.

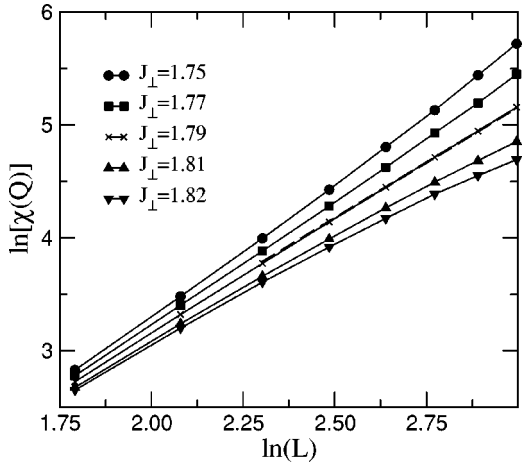

FIG. 9. The finite-size scaling of the staggered $\mathbf{Q}=(\pi,\pi)$ static susceptibility in the vicinity of the critical coupling for $\alpha=0.5$. For lattices larger than $L=10$, the data close to the critical coupling is found to fit a power law behavior with an exponent $2-\eta$ ($\eta=0.035$) that is consistent with the 3D Heisenberg universality class.

$\rho_x(\rho_y)$. From the data, we estimate the true critical coupling in the limit of infinite system size to be $J_\perp^c=1.79\pm0.005$ for $\alpha=0.5$.

A similar analysis of the spin stiffness data for different values of α gives us the critical value of the interplanar coupling $J_\perp^c$ for the spin gap transition as a function of α. The resulting phase diagram is shown in Fig. 1.

Independent estimate of the critical coupling can be obtained from the finite size scaling of the staggered structure factor and the corresponding susceptibility. The full two-plane static spin susceptibility is defined as

$$\chi(\mathbf{q})=\frac{1}{L^2}\sum_{i,j} e^{i\mathbf{q}\cdot(\mathbf{r}_i-\mathbf{r}_j)}\int_0^\beta d\tau\langle[S^z_{1,j}(\tau)-S^z_{2,j}(\tau)][S^z_{1,i}(0)-S^z_{2,i}(0)]\rangle. \tag{12}$$

At the critical point, the staggered, $\mathbf{q}=(\pi,\pi)$, susceptibility for finite size systems scale with the system size as a simple power law behavior[32,33] determined by the critical exponent η:

$$\chi(L,J_\perp^c)\sim L^{2-\eta}. \tag{13}$$

This implies that on a plot of $\ln(\chi)$ versus $\ln(L)$, the data for the critical $J_\perp$ should fall on a straight line with slope $2-\eta$. In the spin gapped phase, the staggered susceptibility should go to a constant at large L, whereas in the Néel phase with long-range antiferromagnetic order, it should diverge faster than any power of L. Figure 9 shows the plot of $\ln(\chi)$ versus $\ln(L)$ for fixed $\alpha(=0.5)$ and five different values of $J_\perp$ in the vicinity of the critical coupling. For large values of L, the data for the critical coupling is indeed found to fall on a straight line. The slope of the line yields $\eta\approx0.035$. The deviation from power law behavior in both the spin gapped and Néel phases are also in agreement with the above discussion. The value of η obtained from Fig. 9 is in close agreement with its value for the 3D Heisenberg universality class. Furthermore, both the staggered structure factor and susceptibility (for any $\alpha>0$) show the expected finite-size scaling with the critical exponents $\nu\approx0.7$ and $\gamma\approx1.4$. This confirms that the transition belongs to the universality class of the 3D Heisenberg model for any finite α.

V. FINITE TEMPERATURE PROPERTIES

A. Uniform susceptibility

We start the presentation of the finite temperature properties with the uniform magnetic susceptibility defined as

$$\chi_u=\frac{\beta}{N}\sum_{i,j}\langle[S^z_{1,i}+S^z_{2,i}][S^z_{1,j}+S^z_{2,j}]\rangle, \tag{14}$$

where N is the size of the system. For finite temperature properties, we have carried out the simulations on lattices with rectangular geometry $L_x\times L_y, L_x\neq L_y$. This is to reduce finite size effects. It was shown by Sandvik[38] for a system of coupled Heisenberg chains, the finite size effects depended monotonically for rectangular lattices whereas for square lattices the behavior was less well behaved. While such effects are expected for ground state properties also, our limitation in terms of computational power has restricted us to the use of square lattices. Fortunately, the stiffness in the two directions give upper and lower bounds for the critical coupling, leading to a reliable estimate of $J_\perp^c$. Simulations at finite temperatures require considerably less computer power—hence we are able to study rectangular lattices. In particular, lattices with aspect ratio $L_x=4L_y$ have been considered.

Results from the study of the nonlinear σ model predict that at the critical coupling, the uniform susceptibility $\chi(T)$ is linear in T (at low temperatures) with zero intercept. The region of linear T dependence gives an estimate of the quantum critical regime. The finite-size effects in the estimates of $T>0$ data decrease rapidly with increasing system size—the difference in the estimate of χ_u between lattices with L_x

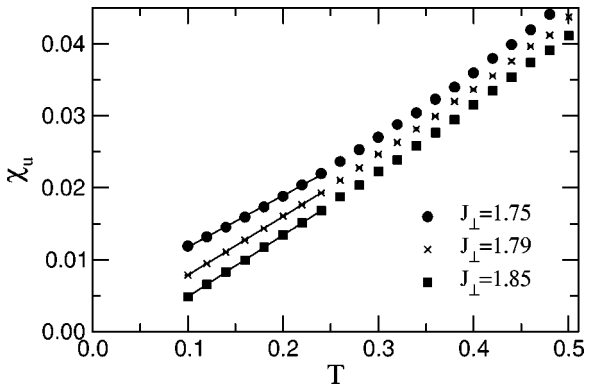

FIG. 10. The uniform susceptibility as a function of temperature near the critical coupling for $\alpha=0.5$. At low temperatures, the susceptibility depends linearly on T, in agreement with the prediction from field theoretic calculations. Above the transition, in the spin gapped phase, χ_u scales to zero at finite T, while below the transition, in the Néel phase, χ_u scales to a finite value at $T=0$. At the critical point, χ_u extrapolates to zero at $T=0$. The data shown are for a rectangular lattice with $N=128\times32$.

$=64$ and 128 is of the order of the magnitude of the error bars up to the lowest temperatures studied. Henceforth, the data are presented for lattices with $L_x=128$. Figure 10 show the temperature dependence of the χ_u for three different values of the inter-planar coupling close to the critical value. The data shown are for a rectangular lattice with $L_x=128$. It was found that the difference in the estimates of χ_u at low temperatures. For all the values, the uniform susceptibility is linear in T over the range of temperature shown. For $J_\perp^c$, the intercept is approximately zero, while it is positive (negative) for $J_\perp<(>)J_\perp^c$. The results are consistent with the estimate of $J_\perp^c$ obtained from the stiffness data. While the linear T behavior at the critical coupling is found to hold for all values of the in-plane spatial anisotropy, its range decreases with decreasing value of α.

B. Internal energy and specific heat

Instead of working directly with the specific heat, we have studied the internal energy, of which the specific heat is the temperature derivative. This is driven by the practical consideration that the specific heat data (that can be estimated directly within the framework of the SSE method) gets noisy at low temperatures, while the internal energy data is largely free from such noise at all temperatures considered. The temperature dependence of the specific heat is easily obtained from that of the internal energy. An estimate of the temperature dependence of the internal energy is obtained by assuming spin wave dispersion at low energies. In the Néel phase, the dispersion is $\varepsilon(k)=ck$, where c is the spin wave velocity. In the presence of a spin gap (Δ), the dispersion takes the form $\varepsilon(k)=\sqrt{\Delta^2+c^2k^2}$. For a 2D system, the internal energy per particle at low temperatures should take the form

$$\frac{E}{N}\sim\int_0^\infty kdk\varepsilon(k)\frac{1}{e^{-\varepsilon(k)/k_BT}-1}.$$

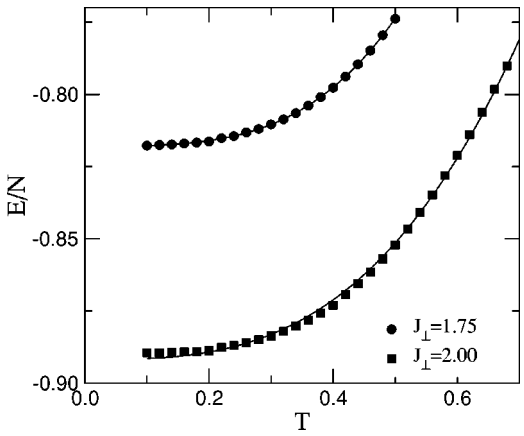

FIG. 11. The energy as a function of the temperature for the Néel and the spin gapped phases. The data for $J_\perp=1.85$ is found to deviate from a pure T^3 dependence at low temperatures.

For the gapless dispersion, this gives $E/N=(\text{const})\times T^3$, which implies that the specific heat $C_v\sim T^2$. For the spin gapped phase, the internal energy expression reduces to

$$\frac{E}{N}=(\text{const})\times T^3\int_{\Delta^2/T}^\infty\frac{x^2dx}{e^x-1}.$$

For $\Delta^2\ll T$, the leading behavior of the specific heat is once again $\sim T^2$. For large gap and/or low temperatures, this will turn into an activated behavior, coming from the temperature dependence of the definite integral. However, this region has not been accessible to our Monte Carlo simulations. Figure 11 shows the internal energy as a function of the temperature for two parameter sets corresponding to the gapless and spin gapped phases along with the T^3 fit. This suggests that unless one goes down to very low temperatures, near the critical line it would be difficult to tell from the specific heat data whether one is in an ordered or a spin-gap phase.

VI. COMPARISON WITH EXPERIMENTS

Let us now consider the two materials $SrCu_2O_3$ and $CaCu_2O_3$. The former has been considered as a model spin-ladder system.[2] It is known to have a spin gap of about 420 K in the excitation spectra.[16] From its geometry, one expects $J_\perp$ comparable to J. Early attempts to study this model used a ladder geometry ($\alpha=0$) with $J_\perp=J$, and concluded[35] that the experimental data can be fit with $J\approx850$ K. Later direct measurements of the susceptibility yielded[36] a much larger value of $J\approx2000$ K. Johnston[37] later suggested that the susceptibility data can be explained (once again with a ladder geometry) with J of order 2000 K and a much smaller $J_\perp$ (less than $0.5J$). However, as pointed out by Greven and Birgeneau,[39] one always expects in these materials, an inter-ladder coupling in the third direction leading to a nonzero α, possibly as large as $\alpha\approx0.05$. Our study shows that even this small a value of α, along with $J_\perp=0.5$ would push Sr_2CuO_3 into the Néel phase. To account for the experimentally observed spin-gapped behavior with $\alpha\approx0.05$ one needs $J_\perp/J\sim1.0$. We have indicated this in Fig. 1. The main difference

between $SrCu_2O_3$ and $CaCu_2O_3$ is that in the latter buckling leads to much smaller $J_\perp/J(\approx 0.2)$ (Ref. 14) thus leading to Néel order. This is also indicated in the phase diagram in Fig. 1.

VII. CONCLUSIONS

We have used the stochastic series expansion (SSE) quantum Monte Carlo (QMC) and series expansion methods to study the antiferromagnetic Heisenberg model on spatially anisotropic bilayer systems. The critical $J_\perp^c$, separating the Néel ordered and disordered phases is found to depend on α, the ratio of in-plane couplings, according to a simple square-root behavior. For all values of α considered, the transition to the spin-gapped state belongs to the universality class of the 3D classical Heisenberg model. The $T=0$ and finite temperature properties of the model are studied, especially around the critical line. We find that the spin-wave spectra evolve smoothly through the transition. The spin-wave velocity becomes highly anisotropic as $\alpha \to 0$. We hope our work would stimulate further measurements of spin-wave spectra for materials such as $SrCu_2O_3$ and $CaCu_2O_3$.

ACKNOWLEDGMENTS

We would like to thank H. Rosner, A. Sandvik, J. Oitmaa, and C.J. Hamer for fruitful discussions. This work was supported in part by the US National Science Foundation Grant Nos. DMR-9986948 and DMR-0240918 and by the Australian Research Council. Part of the simulations were carried out on the IBM SP facility at NERSC. We are also grateful for the computing resources provided by the Australian Partnership for Advanced Computing (APAC) National Facility.

*Present address: Department of Physics, University of California, Riverside, California 92521, USA; Electronic address: pinaki@physics.ucr.edu
†Electronic address: w.zheng@unsw.edu.au
‡Electronic address: singh@physics.ucdavis.edu

[1] R.R.P. Singh, W.E. Pickett, D.W. Hone, and D.J. Scalapino, Comments Mod. Phys., Part C **2**, N1:B1 (2000).
[2] E. Dagotto and T.M. Rice, Science **271**, 618 (1996).
[3] Y.J. Kim, A. Aharony, R.J. Birgeneau, F.C. Chou, O. Entin-Wohlman, R.W. Erwin, M. Greven, A.B. Harris, M.A. Kastner, I. Ya. Korenbilt, Y.S. Lee, and G. Shirane, Phys. Rev. Lett. **83**, 852 (1999).
[4] See for example, H. Kageyama, K. Yoshimura, R. Stern, N.V. Mushnikov, K. Onizuka, M. Kato, K. Kosuge, C.P. Slichter, T. Goto, and Y. Ueda, Phys. Rev. Lett. **82**, 3168 (1999).
[5] S. Chakravarty, B.I. Halperin, and D.R. Nelson, Phys. Rev. B **39**, 2344 (1989).
[6] A.V. Chubukov, S. Sachdev, and J.Y. Ye, Phys. Rev. B **49**, 11 919 (1994).
[7] I. Affleck, *Proceedings of the Les Houches Summer School*, session XLIX, edited by E. Brezin and J. Zinn-Justin (North Holland, Amsterdam, 1988).
[8] A.O. Gogolin, A.A. Nersesyan, and A.M. Tsvelik, *Bosonization and Strongly Correlated Systems* (Cambridge University Press, Cambridge, U.K. 1998).
[9] S.R. White, Phys. Rev. Lett. **69**, 2863 (1992).
[10] J. Oitmaa, R.R.P. Singh, and W.H. Zheng, Phys. Rev. B **54**, 1009 (1996).
[11] I. Affleck and B.I. Halperin, J. Phys. A **29**, 2627 (1996); I. Affleck, M.P. Gelfand, and R.R.P. Singh, *ibid.* **27**, 7313 (1994).
[12] O.A. Starykh, R.R.P. Singh, and G.C. Levine, Phys. Rev. Lett. **88**, 167203 (2002).
[13] R. Coldea, D.A. Tennant, A.M. Tsvelik, and Z. Tylczynski, Phys. Rev. Lett. **86**, 1335 (2001).
[14] V. Kiryukhin *et al.*, Phys. Rev. B **63**, 144418 (2001).
[15] H. Rosner (private communication).
[16] M. Azuma, Z. Hiroi, M. Takano, K. Ishida, and Y. Kitaoka, Phys. Rev. Lett. **73**, 3463 (1994).
[17] J.H. Schön, M. Dorget, F.C. Beuran, X.Z. Xu, E. Arushanov, M. Laguës, and C. Deville Cazvellin, Science **293**, 2430 (2001).
[18] See, for example, A.W. Sandvik and D.J. Scalapino, Phys. Rev. Lett. **72**, 2777 (1994); M. Troyer and S. Sachdev, *ibid.* **81**, 5418 (1998); P.V. Shevchenko, A.W. Sandvik, and O.P. Sushkov, Phys. Rev. B **61**, 3475 (2000), and references cited therein.
[19] M.P. Gelfand and R.R.P. Singh, Adv. Phys. **49**, 93 (2000).
[20] K. Hida, J. Phys. Soc. Jpn. **61**, 1013 (1992).
[21] M.P. Gelfand, Phys. Rev. B **53**, 11 309 (1996).
[22] W. Zheng, Phys. Rev. B **55**, 12 267 (1997).
[23] A.W. Sandvik and J. Kurkijärvi, Phys. Rev. B **43**, 5950 (1991); A.W. Sandvik, *ibid.* **56**, 11 678 (1997).
[24] A.W. Sandvik, Phys. Rev. B **59**, R14 157 (1999).
[25] O.F. Syljuåsen and A.W. Sandvik, Phys. Rev. E **66**, 046701 (2002).
[26] A.J. Guttmann, in *Phase Transitions and Critical Phenomena*, edited by C. Domb and J. Lebowitz (Academic, New York, 1989), Vol. 13.
[27] W. Kohn, Phys. Rev. **133**, A171 (1964).
[28] P. Kopietz, Phys. Rev. B **57**, 7829 (1998).
[29] E.L. Pollock and D.M. Ceperley, Phys. Rev. B **36**, 8343 (1987).
[30] K. Harada and N. Kawashima, Phys. Rev. B **55**, R11 949 (1998).
[31] A. Cuccoli, T. Roscilde, V. Tognetti, R. Vaia, and P. Verrucchi, cond-mat/0209316 (unpublished).
[32] M. Wallin, E.S. Sørensen, S.M. Girvin, and A.P. Young, Phys. Rev. B **49**, 12 115 (1994).
[33] For a review of finite-size scaling, see M.N. Barber, in *Phase Transitions and Critical Phenomena*, edited by Domb and Lebowitz (Academic Press, New York, 1983), Vol. 8.
[34] We would like to thank Anders Sandvik for suggesting such a finite-size behavior of the stiffness along the two principal axes.
[35] A.W. Sandvik, E. Dagotto, and D.J. Scalapino, Phys. Rev. B **53**, 2934 (1996).
[36] N. Motoyama, H. Eisaki, and S. Uchida, Phys. Rev. Lett. **76**, 3212 (1996).
[37] D.C. Johnston, Phys. Rev. B **54**, 13009 (1996).
[38] A.W. Sandvik, Phys. Rev. Lett. **83**, 3069 (1999).
[39] M. Greven and R.J. Birgeneau, Phys. Rev. Lett. **81**, 1945 (1998).